

Structures and correlation functions of multicomponent and polydisperse hard-sphere mixtures from a density functional theory

Yang-Xin Yu^{a)}

Department of Chemical Engineering, Tsinghua University, Beijing 100084, People's Republic of China
and State Key Laboratory of Chemical Engineering, Tsinghua University, Beijing 100084,
People's Republic of China

Jianzhong Wu

Department of Chemical and Environmental Engineering, University of California, Riverside,
California 92521-0425

Yu-Xuan Xin and Guang-Hua Gao

Department of Chemical Engineering, Tsinghua University, Beijing 100084, People's Republic of China

(Received 15 March 2004; accepted 23 April 2004)

The structures of nonuniform binary hard-sphere mixtures and the correlation functions of uniform ternary hard-sphere mixtures were studied using a modified fundamental-measure theory based on the weight functions of Rosenfeld [Rosenfeld, *Phys. Rev. Lett.* **63**, 980 (1989)] and Boublik-Mansoori-Carnahan-Starling-Leland equation of state [Boublik, *J. Chem. Phys.* **53**, 471 (1970); Mansoori *et al.*, *J. Chem. Phys.* **54**, 1523 (1971)]. The theoretical predictions agreed very well with the molecular simulations for the overall density profiles, the local compositions, and the radial distribution functions of uniform as well as inhomogeneous hard-sphere mixtures. The density functional theory was further extended to represent the structure of a polydisperse hard-sphere fluid near a hard wall. Excellent agreement was also achieved between theory and Monte Carlo simulations. The density functional theory predicted oscillatory size segregations near a hard wall for a polydisperse hard-sphere fluid of a uniform size distribution. © 2004 American Institute of Physics. [DOI: 10.1063/1.1763142]

I. INTRODUCTION

Hard-sphere (HS) model plays a central role in studying the microscopic structures of soft condensed materials using statistical mechanics. It provides not only a good representation of colloidal dispersions¹ where the range of interparticle attraction is typically much smaller than the particle size but also an excellent reference for studying the properties of simple liquids where the structure is predominately determined by the short-ranged repulsion.² Conventionally the correlation functions of a uniform hard-sphere fluid are represented by the Percus-Yevick (PY) integral-equation theory³ while various density functional theories (DFT) (Ref. 4) have been proposed to represent the structures of inhomogeneous hard spheres. Both approaches are highly accurate for one-component hard-sphere systems and multicomponent mixtures. However, their applications for predicting the structures of polydisperse hard spheres as of interest for many colloidal applications are more challenging.^{5,6} The integral-equation approach has been applied to predicting the structure of a uniform polydisperse hard-sphere fluid⁷ and the phase diagram of polydisperse hard-sphere mixtures.⁸ A similar approach was implemented to predict the structure of a polydisperse fluid near a hard wall using a singlet-type integral-equation theory.⁹ DFT has also been employed to study the structures of nonuniform multicomponent

mixtures^{10,11} and polydisperse hard spheres.^{5,12} Using the test-particle method, DFT can also be used to predict the structures of hard-sphere mixtures or polydisperse hard spheres at uniform conditions.^{11,13,14}

The central task of a DFT approach is to construct a reasonably accurate Helmholtz energy functional for the system under consideration. This functional is usually constructed using known structural or thermodynamic information for the corresponding bulk fluids. Two common approaches have been used to develop the approximate Helmholtz functionals.¹⁵ One is based on the functional perturbation expansion with respect to a reference fluid¹⁶ and the other follows the so-called weighted-density approximation (WDA). Many versions exist for both approaches.^{17–21} Early applications of DFT for hard spheres are primarily based on WDA for pure inhomogeneous fluids; substantial efforts had been made to extend these approaches to multicomponent or polydisperse mixtures. For example, Tan *et al.*²² simplified Tarazona's DFT (Ref. 17) and developed a semiempirical free-energy functional for an inhomogeneous binary hard-sphere mixture. Denton and Ashcroft²³ generalized the WDA of Curtin and Ashcroft¹⁸ and applied it to the structure of binary HS mixture near a wall. Kim *et al.*²⁴ presented a hybrid WDA for nonuniform mixtures. Patra²⁵ applied the method of decoupling of the weight function for mixtures. To avoid time-consuming calculations, most DFT for hard-sphere mixtures adopted computationally simple versions of WDA and subsequently, less accurate density and

^{a)} Author to whom correspondence should be addressed. Electronic mail: yangxyu@mail.tsinghua.edu.cn

concentration profiles were obtained. Using the second-order direct correlation function and the bridge function of the bulk fluid mixture as an input, Patra and Ghosh^{10,11} recently proposed a self-consistent DFT and applied it to studying the structures of binary and ternary hard-sphere mixtures. Implementation of this DFT is coupled with the solution of the Ornstein-Zernike (OZ) integral equation using the thermodynamically consistent Rogers-Young closure.²⁶

The fundamental measure theory (FMT) originally proposed by Rosenfeld²⁰ and a simplified version proposed by Kierlik and Rosinberg²¹ distinguish from most other DFTs of hard-sphere fluids because they are directly applicable to multicomponent systems.²⁷ FMT assumes that the excess Helmholtz energy functional can be expressed in terms of the weighted densities that take into account the geometric features of a spherical particle. Because the weight functions are independent of density distributions, FMT is numerically more convenient than most other WDA. FMT has been previously extended to studying the structure of a polydisperse fluid in the presence of a hard wall^{5,12} and in contact with a semipermeable membrane.²⁸ However, in the original FMT, the Helmholtz energy functional is based on the PY approximation and it overestimates the contact values of density distributions. To overcome this disadvantage, Yu and Wu,¹³ and independently Roth *et al.*²⁹ proposed a modified version of FMT using the Boublik-Mansoori-Carnahan-Starling-Leland (BMCSL) (Ref. 30) equation of state as the input. The modified FMT improves both density distributions and the adsorption isotherms of HS near a hard wall¹³ or in microchannels,³¹ especially at high packing densities. In this work, we apply the modified FMT to studying the structures of binary HS mixtures near a planar hard surface as well as the radial distribution functions of uniform ternary HS mixtures. In addition, we extend the modified FMT to inhomogeneous polydisperse HS fluids.

The rest of this paper is organized as follows. In Sec. II we briefly present the modified FMT for multicomponent and polydisperse HS systems. The results for the density and concentration profiles, radial distribution functions, and local size segregation will be presented and discussed in Sec. III. Some conclusions will be made in Sec. IV.

II. DENSITY FUNCTIONAL THEORY (DFT)

A. DFT for multicomponent systems

We consider an N -component mixture of hard spheres at given temperature T , total volume V , chemical potential μ_i , and external potential $\psi_i(\mathbf{r})$ ($i=1,2,\dots,N$). The grand potential Ω is related to the Helmholtz free-energy functional through a Legendre transform

$$\Omega[\{\rho_i(\mathbf{r})\}] = F[\{\rho_i(\mathbf{r})\}] + \sum_{i=1}^N \int d\mathbf{r} \rho_i(\mathbf{r}) [\psi_i(\mathbf{r}) - \mu_i], \quad (1)$$

where $\{\rho_i(\mathbf{r})\}$ is a set of density distributions. The Helmholtz free-energy functional can be decomposed into ideal-gas and excess parts. The ideal-gas part is known exactly,

$$F^{\text{id}} = k_B T \sum_{i=1}^N \int d\mathbf{r} \rho_i(\mathbf{r}) [\ln(\rho_i(\mathbf{r}) \lambda_i) - 1], \quad (2)$$

where $\lambda_i = (h^2/2\pi m_i k_B T)^{1/2}$ is the thermal wavelength of component i and k_B is the Boltzmann constant. As in the original fundamental measure theory, the excess part of Helmholtz free-energy functional is assumed to be

$$F^{\text{ex}} = k_B T \int \Phi^{\text{hs}}[n_\alpha(\mathbf{r})] d\mathbf{r}, \quad (3)$$

where $\Phi^{\text{hs}}[n_\alpha(\mathbf{r})]$ is the reduced excess Helmholtz free-energy density. The weight density $n_\alpha(\mathbf{r})$ is defined as

$$n_\alpha(\mathbf{r}) = \sum_{i=1}^N \int \rho_i(\mathbf{r}') w^{(\alpha)}(|\mathbf{r}' - \mathbf{r}|, \sigma_i), \quad (4)$$

where σ_i is the diameter of component i and α ($=0, 1, 2, 3, V1, \text{ and } V2$) denote the index of six weight functions given by

$$w^{(3)}(r, \sigma) = \theta(\sigma/2 - r), \quad (5)$$

$$w^{(2)}(r, \sigma) = \delta(\sigma/2 - r), \quad (6)$$

$$w^{(0)}(r, \sigma) = w^{(2)}(r, \sigma) / \pi \sigma^2, \quad (7)$$

$$w^{(1)}(r, \sigma) = w^{(2)}(r, \sigma) / 2\pi \sigma, \quad (8)$$

$$\mathbf{w}^{(V2)}(\mathbf{r}, \sigma) = (\mathbf{r}/r) \delta(\sigma/2 - r), \quad (9)$$

$$\mathbf{w}^{(V1)}(\mathbf{r}, \sigma) = \mathbf{w}^{(V2)}(\mathbf{r}, \sigma) / 2\pi \sigma, \quad (10)$$

where $\delta(r)$ is the Dirac delta function and $\theta(r)$ is the Heaviside step function.

As proposed by Yu and Wu,¹³ the HS Helmholtz free-energy density can be expressed in terms of contributions from scalar weighted densities (S) and vector weighted densities (V)

$$\Phi^{\text{hs}}[n_\alpha] = \Phi^{\text{hs}(S)}[n_\alpha] + \Phi^{\text{hs}(V)}[n_\alpha]. \quad (11)$$

The scalar part according to the modified FMT (Ref. 13) is given by

$$\begin{aligned} \Phi^{\text{hs}(S)}[n_\alpha(\mathbf{r})] = & -n_0 \ln(1 - n_3) + \frac{n_1 n_2}{1 - n_3} + \frac{n_2^3 \ln(1 - n_3)}{36\pi n_3^2} \\ & + \frac{n_2^3}{36\pi n_3 (1 - n_3)^2} \end{aligned} \quad (12)$$

and the vector part by

$$\begin{aligned} \Phi^{\text{hs}(V)}[n_\alpha(\mathbf{r})] = & -\frac{\mathbf{n}_{V1} \cdot \mathbf{n}_{V2}}{1 - n_3} - \frac{n_2 \mathbf{n}_{V2} \cdot \mathbf{n}_{V2}}{12\pi n_3^2} \ln(1 - n_3) \\ & - \frac{n_2 \mathbf{n}_{V2} \cdot \mathbf{n}_{V2}}{12\pi n_3 (1 - n_3)^2}. \end{aligned} \quad (13)$$

In the limit of a bulk fluid, the two vector weighted densities \mathbf{n}_{V1} and \mathbf{n}_{V2} vanish, and the Helmholtz free-energy density Φ^{hs} becomes identical to that from the BMCSL equation of state.³⁰ Although some recent modifications are known to give a better description for the solid phase, these modifications³² would not be more accurate for the fluid phase.

Given the fixed external potential $\psi_i(\mathbf{r})$ and the excess Helmholtz energy functional F^{ex} , the equilibrium density profile $\rho_i(\mathbf{r})$ can be obtained by solving the coupled integral equations that are derived from the minimization of the grand potential functional Ω with respect to $\rho_i(\mathbf{r})$, i.e.,

$$\rho_i(\mathbf{r}) = \rho_i^b \exp \left\{ \beta \mu_i^{\text{ex}} - \beta \sum_{\alpha} \int \frac{\partial \Phi}{\partial n_{\alpha}} w^{(\alpha)}(|\mathbf{r}' - \mathbf{r}|, \sigma_i) d\mathbf{r}' - \beta \psi_i(\mathbf{r}) \right\} \quad (i = 1, 2, \dots, N), \quad (14)$$

where $\beta = 1/k_B T$, ρ_i^b and μ_i^{ex} are the bulk density and the residue chemical potential of component i , respectively. For the bulk fluid, the residue chemical potential is obtained from the BMCSL equation of state. Equation (14) can be solved numerically using the Picard-type iterative method where the weighted densities and integrals are evaluated using a trapezoidal rule. To avoid divergence, it is necessary to mix the new and old density profiles in certain proportions during the iteration process, i.e.,

$$\rho_{\text{in}}^{(i)}(\mathbf{r}) = \rho_{\text{out}}^{(i-1)}(\mathbf{r})f + \rho_{\text{in}}^{(i-1)}(\mathbf{r})(1-f), \quad (15)$$

where f is the mixing parameter obtained by trial and error method. We find that a mesh of $0.01\sigma_1$ yields satisfactory numerical accuracy (maximum difference of density profiles between two iteration is $\Delta\rho_i = 1 \times 10^{-5}$). The time required to solve Eq. (14) depends on the diameter ratios, initial values of density profiles, and mixing parameter. For example, when we compute the density profiles of a binary hard-sphere mixture ($\sigma_2/\sigma_1 = 3$, $x_1^b = 0.2856$, and $\eta = 0.656$) near a hard wall on a PC (with CPU Athlon XP 1800, System memory 256MB DDR SDRAM), 4.25 min is required in the condition of $f = 0.03$ (in the first three iterations $f = 0.00008$) and using bulk densities as initial values of density profiles. For ternary and polydisperse systems, more computation time is needed.

B. Inhomogeneous polydisperse system

The structure of an inhomogeneous polydisperse HS fluid can be specified by the local number density profile, $\rho(\mathbf{r}, \sigma)$, of each species with the diameter σ . In the bulk limit, the system is characterized by the particle size distribution given by a normalized probability function $f(\sigma)$. The bulk density of particle with the diameter σ is expressed as

$$\rho^b(\sigma) = \rho_0^b f(\sigma). \quad (16)$$

The weighted densities for the inhomogeneous polydisperse fluid can be simply generalized from Eq. (4)

$$n_{\alpha}(\mathbf{r}) = \int d\sigma d\mathbf{r}' \rho(\mathbf{r}') w^{(\alpha)}(|\mathbf{r}' - \mathbf{r}|, \sigma), \quad (17)$$

where $w^{(\alpha)}(|\mathbf{r}' - \mathbf{r}|, \sigma)$ is given in Eqs. (5)–(10). With these descriptions, the grand potential becomes

$$\begin{aligned} \Omega = & k_B T \int d\sigma d\mathbf{r} \rho(\mathbf{r}, \sigma) \{ \ln[\lambda^3(\sigma)\rho(\mathbf{r}, \sigma)] - 1 \} \\ & + k_B T \int d\mathbf{r} \Phi^{\text{bs}}[n_{\alpha}(\mathbf{r})] + \int d\sigma d\mathbf{r} [\psi(\mathbf{r}, \sigma) \\ & - \mu(\sigma)] \rho(\mathbf{r}, \sigma), \end{aligned} \quad (18)$$

where $\mu(\sigma)$ and $\lambda(\sigma)$ are, respectively, the chemical potential and the thermal wavelength of species with the diameter σ . Minimization of Eq. (18) leads to the Euler-Lagrange equation for the inhomogeneous polydisperse fluid,

$$\begin{aligned} \rho(\mathbf{r}, \sigma) = & \rho_0^b f(\sigma) \exp \left[\mu^{\text{ex}}(\sigma) - \beta \psi(\mathbf{r}, \sigma) \right. \\ & \left. - \sum_{\alpha} \int d\mathbf{r}' \frac{\partial \Phi^{\text{bs}}}{\partial n_{\alpha}} w^{(\alpha)}(|\mathbf{r}' - \mathbf{r}|, \sigma) \right], \end{aligned} \quad (19)$$

where $\mu^{\text{ex}}(\sigma)$ is the residue chemical potential of species with the diameter σ in bulk limit. Both the trapezoidal rule and the Gauss quadrature method, as proposed by Pizio *et al.*,¹² can be employed to evaluate the weighted densities and the integral in Eq. (19), but the latter is more efficient. If the external potential $\psi(\mathbf{r}, \sigma)$ (such as a hard wall) and the polydispersity of bulk limit are known in advance, Eqs. (11)–(13), (17), and (19) are closed and their numerical solution gives the full density profile of nonuniform polydisperse hard-sphere fluid.

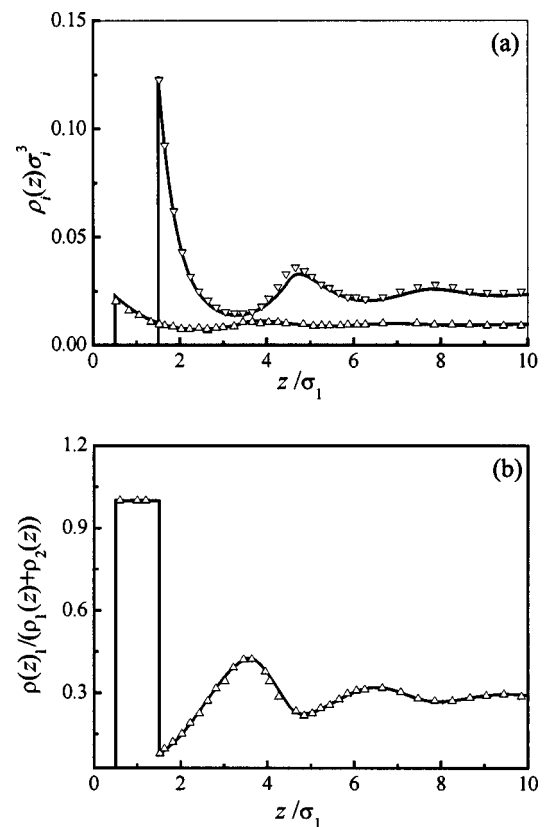


FIG. 1. (a) Density profiles and (b) local concentration of a binary hard-sphere mixture near a hard wall for the diameter ratio $\sigma_2/\sigma_1 = 3.0$, bulk molar fraction $x_1^b = 0.2856$, and bulk packing fraction $\eta = 0.656$. Symbols are simulation results (Ref. 22) and the solid curves are results from the modified FMT.

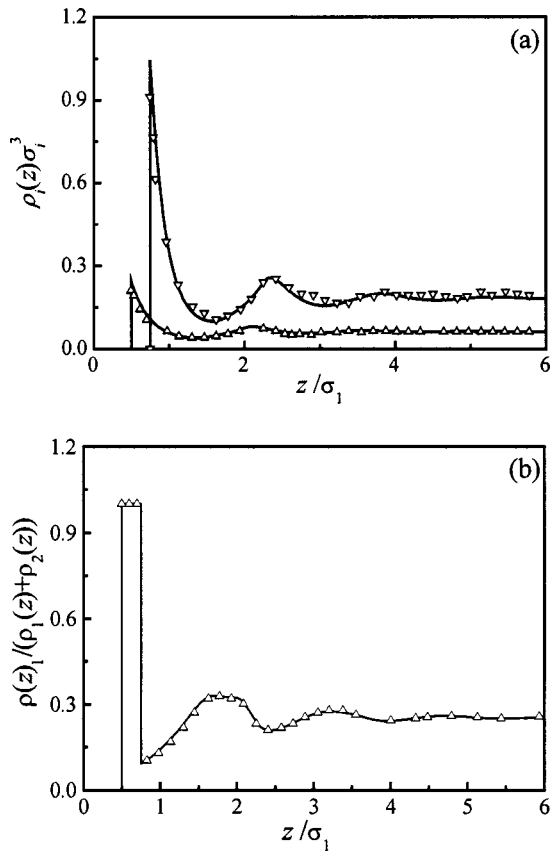


FIG. 2. The same as Fig. 1 but for the diameter ratio $\sigma_2/\sigma_1=1.5$, bulk molar fraction $x_1^b=0.2538$, and bulk packing fraction $\eta=0.682$.

III. RESULTS AND DISCUSSION

A. Hard-sphere mixtures near a hard wall

We first investigate the structures of binary hard-sphere mixtures near a flat hard wall. In this case, the external potential acting on each particle i can be expressed as

$$\psi_i(z) = \begin{cases} \infty & z < \sigma_i/2 \\ 0 & z > \sigma_i/2 \end{cases} \quad (20)$$

where z is the perpendicular distance from the wall. The bulk conditions used in the calculations are specified by the ratio of the hard-sphere diameters, the packing fraction η defined as

$$\eta = \frac{\pi}{6} \sum_{i=1}^N \rho_i^b \sigma_i^3, \quad (21)$$

and the mole fraction x_i^b . In all our calculations, σ_1 is selected as the unit length.

Figures 1(a) and 1(b) present, respectively, the density and mole fraction profiles near a hard wall for a binary HS mixture of $\sigma_2/\sigma_1=3.0$, $\eta=0.656$, and $x_1^b=0.2856$. For comparison, the computer simulation results of Tan *et al.*²² are also included in both figures. As in a pure HS fluid, the density profiles oscillate with a periodicity of a hard-sphere diameter σ_i and approach the corresponding bulk densities far away from the wall. It shows that the higher the reduced bulk density is, the larger is the magnitude of oscillation in the density profile. It can be seen from these figures that the

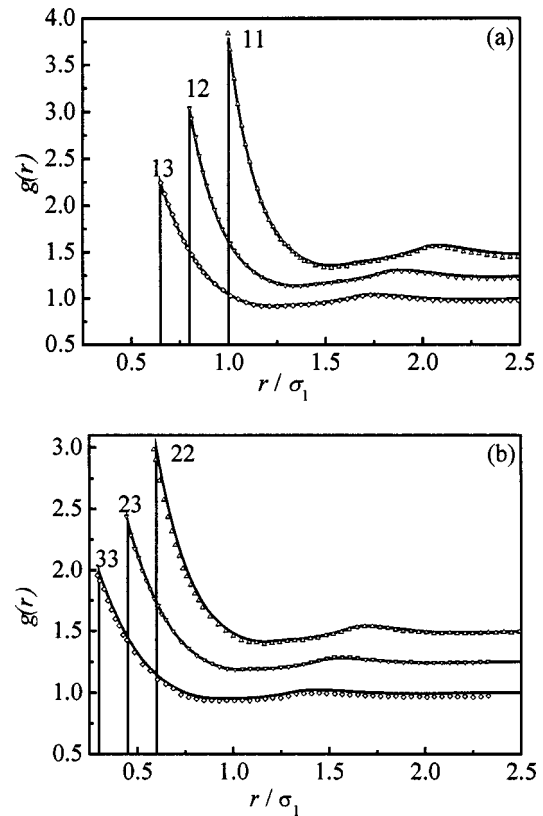


FIG. 3. Radial distribution functions of a ternary hard-sphere mixture with $\sigma_2/\sigma_1=0.6$, $\sigma_3/\sigma_1=0.3$, $x_1=x_2=x_3=1/3$, and $\eta=0.35$. The symbols represent the results of MC simulation (Ref. 33) and the solid curves are predicted from the modified FMT. For clarity, curves for $g_{12}(r)$ and $g_{23}(r)$, and for $g_{11}(r)$ and $g_{22}(r)$ are shifted upward by 0.25 and 0.5, respectively.

present DFT accurately predicts the density and mole fraction profiles. Previous DFT investigations also yield good overall density profiles but the local mole fractions are less satisfactory.^{22–25} For a binary HS mixture at $\sigma_2/\sigma_1=1.5$, $\eta=0.682$, and $x_1^b=0.2538$, similar results can be found in Fig. 2. In both cases, surface segregation is observed and well reproduced by the present DFT.

B. Structures of ternary hard-sphere mixtures

Using Percus' test-particle method, DFT can be used to calculate the radial distribution functions of bulk mixtures. If we fix a sphere i and obtain the density profile $\rho_j(r)$ of component j around the fixed particle, the radial distribution function $g_{ji}(r)$ can be obtained through

$$g_{ji}(r) = \rho_j(r) / \rho_j^b. \quad (22)$$

Equation (22) has been applied to ternary hard-sphere mixtures with the diameter ratios of $\sigma_2/\sigma_1=0.6$ and $\sigma_3/\sigma_1=0.3$. Figure 3 depicts the predicted radial distribution functions for the ternary system at $x_1=x_2=x_3=1/3$ and $\eta=0.35$, along with the Monte Carlo data of Sindelka and Boublík.³³ The agreement between the DFT and the computer simulation is excellent. The contact values of the radial distribution functions from the present DFT are same as those from the BMCSL equation of state, indicating the consistency of the DFT. We have performed similar calculations for other ternary systems by changing the concentration and

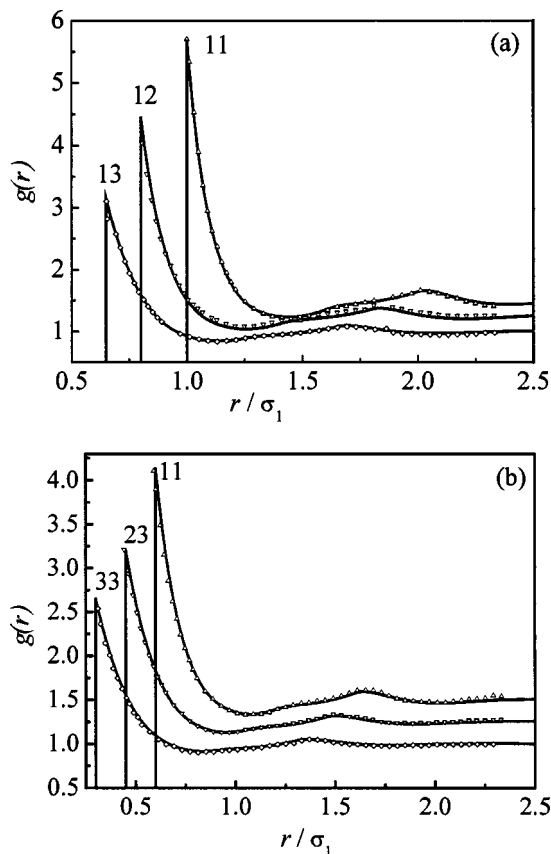


FIG. 4. Radial distribution functions of a ternary hard-sphere mixture as in Fig. 3 but for $\eta=0.45$.

the overall packing fraction. The predicted results are shown in Figs. 4–6, all are in excellent agreement with the simulation data.³³ As the reduced density increases, the oscillations in the radial distribution function profiles magnify, similar to the distribution of hard spheres near a hard wall.

We have taken an alternative way to calculate the radial distribution functions from the second direct correlation functions obtained from the functional derivatives of the excess Helmholtz energy functional

$$C_{ij}^{(2)}(|\mathbf{r}''-\mathbf{r}'|) = -\frac{\beta \delta^2 F^{\text{ex}}[\{\rho_i(\mathbf{r})\}]}{\delta \rho_i(\mathbf{r}'') \delta \rho_j(\mathbf{r}')}. \quad (23)$$

The total correlation functions $h_{ij}(r) = g_{ij}(r) - 1$ are calculated from the Ornstein-Zernike (OZ) equation via the Fourier transform. However, this route is less accurate than Percus' test-particle method for the radial distribution functions. Therefore, only the latter method is used throughout this paper although the present DFT predicts the direct correlation functions more accurately than the original FMT.

C. Polydisperse fluid near a hard wall

We now apply the DFT to polydisperse hard spheres with a special attention given to the effect of a hard wall on the fluid structure. The polydispersity may be specified by a Gaussian, exponential, or a uniform probability distribution function for the particle size. In this work, we focus on a uniform distribution function $f(\sigma)$ within the interval $[\sigma_1, \sigma_u]$,

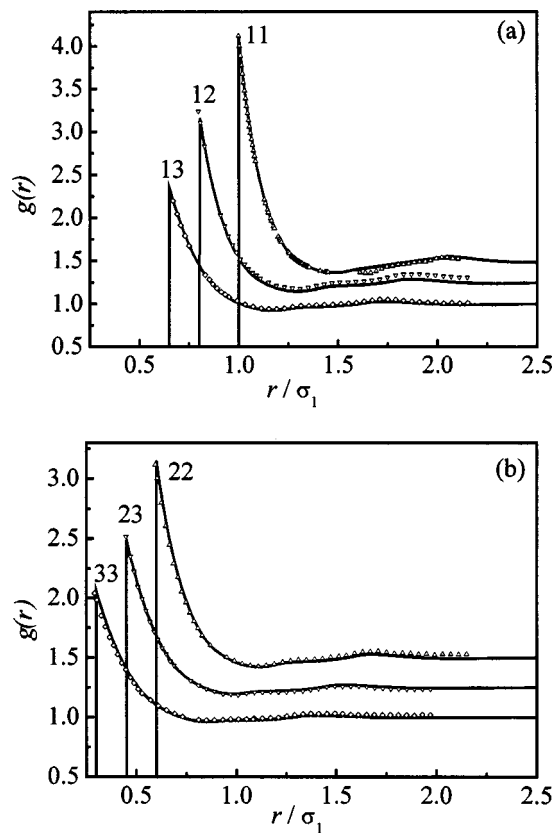


FIG. 5. Radial distribution functions of a ternary hard-sphere mixture as in Fig. 3 but for $x_1=1/6, x_2=1/3, x_3=1/2$, and $\eta=0.35$.

$$f(\sigma) = \begin{cases} \frac{1}{\sigma_1 - \sigma_u} & \sigma_1 < \sigma < \sigma_u \\ 0 & \text{otherwise} \end{cases}, \quad (24)$$

and the fluid is in contact with a planar hard wall. The external potential for the particle with a diameter σ is expressed as

$$\psi(z, \sigma) = \begin{cases} \infty & z < \sigma/2 \\ 0 & z \geq \sigma/2 \end{cases}. \quad (25)$$

Figure 7 compares the density profiles of the smallest ($\sigma = \sigma_1$) and the largest ($\sigma = \sigma_u = 2\sigma_1$) particles predicted from the DFT with that from Monte Carlo simulations at two bulk densities ($\rho_{0b}\sigma_1^3 = 0.0908$ and $\rho_{0b}\sigma_1^3 = 0.181$). At the fixed bulk density ρ_{0b} , the oscillation in the density profiles becomes more pronounced as the particle size increases. The agreement between the theoretical predictions and the Monte Carlo simulations is very good, indicating that the present DFT is capable of predicting the structure of the inhomogeneous polydisperse hard spheres with high accuracy. Comparing with Fig. 1 of Ref. 12, we find that the present DFT is slightly more accurate than those used by Pizio *et al.*¹² and by Pagonabarraga *et al.*⁵

A three-dimensional plot of the density profile as a function of particle diameter and the distance from the hard wall is shown in Fig. 8, where the bulk condition is same as in Fig. 7(b). This plot illustrates that the local density changes continuously with the diameter of the adsorbed particles. The

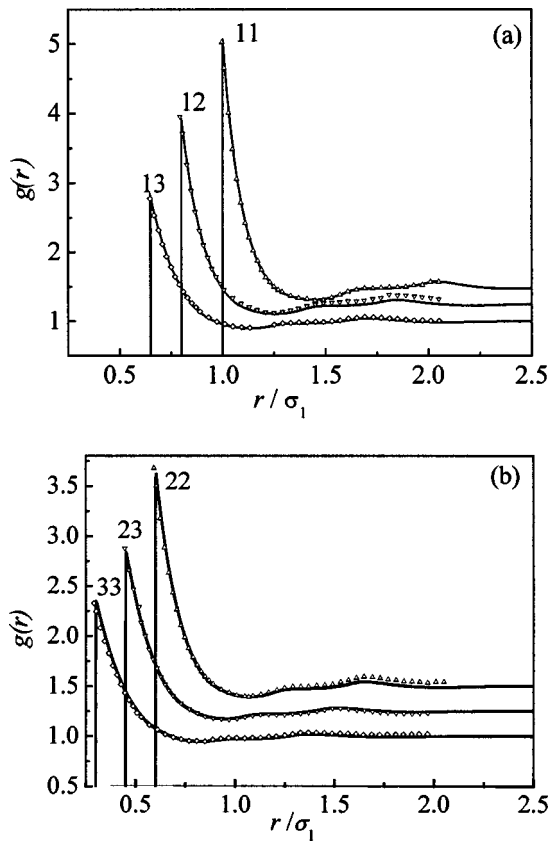


FIG. 6. Radial distribution functions of a ternary hard-sphere mixture as in Fig. 3 but for $x_1=1/6$, $x_2=1/3$, $x_3=1/2$, and $\eta=0.4$.

contact density of particles shows oscillatory behavior as the particle size increases. Although here we only considered the polydisperse fluid systems with uniform size distribution, our method is feasible to the case with nonlinear distribution of diameters.

Significant local size segregation was found for the polydisperse fluid with uniform size distribution as discussed in Figs. 7 and 8. Figure 9 depicts the local mole fraction profiles, $x(z, \sigma) = \rho(z, \sigma) / \int d\sigma \rho(z, \sigma)$, for the system with the size distribution given by Eq. (24) and the bulk density $\rho_{0b}\sigma_1^3 = 0.24$. It can be clearly seen from Fig. 9 that the density profile of each species oscillates with a spatial period close to its own diameter. This behavior is similar to that in binary and ternary mixtures as discussed earlier. In addition, strong oscillations in the local concentration profiles are found for the large and small particles, whereas for the particles close to the mean size ($\sigma = 1.4\sigma_1$ and $\sigma = 1.6\sigma_1$), the concentration profiles are more uniform. These findings are qualitatively in coincidence with the predicted results obtained by Pagonabarraga *et al.*⁵

IV. CONCLUSIONS

We have applied the modified fundamental measure theory to inhomogeneous as well as uniform multicomponent (binary and ternary) hard-sphere mixtures and polydisperse systems. Extensive comparison with Monte Carlo simulation results indicates that the modified fundamental measure theory accurately reproduces the density profiles as well as

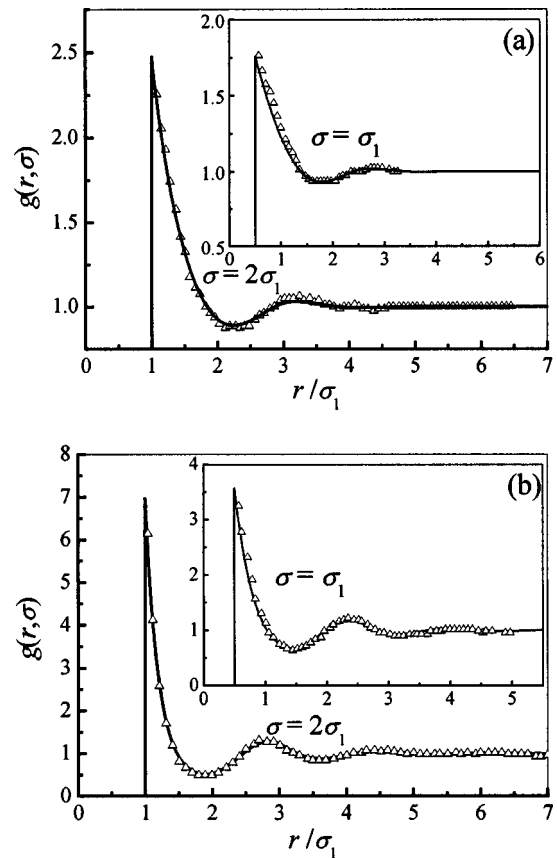


FIG. 7. Reduced density profiles for particles of diameter $\sigma = \sigma_1$ and $\sigma = 2\sigma_1$ for polydisperse hard spheres near a hard wall at bulk density (a) $\rho_{0b}\sigma_1^3 = 0.0908$ and (b) $\rho_{0b}\sigma_1^3 = 0.181$. The symbols represent the results of MC simulation (Ref. 12) and the solid curves are calculated from the DFT.

the radial distribution functions of hard-sphere mixtures, and the predicted results are better than the previous versions of the density functional theory.^{22–25} The present theory works successfully not only at high densities but also for highly

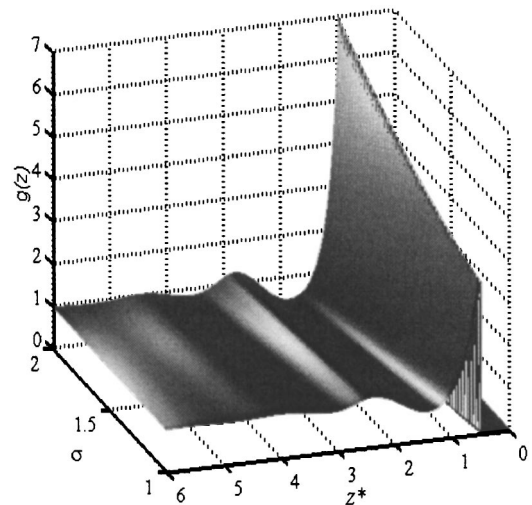


FIG. 8. The reduced density distribution of polydisperse hard spheres vs particle diameter and the perpendicular distance from the wall at the bulk density $\rho_{0b}\sigma_1^3 = 0.181$.

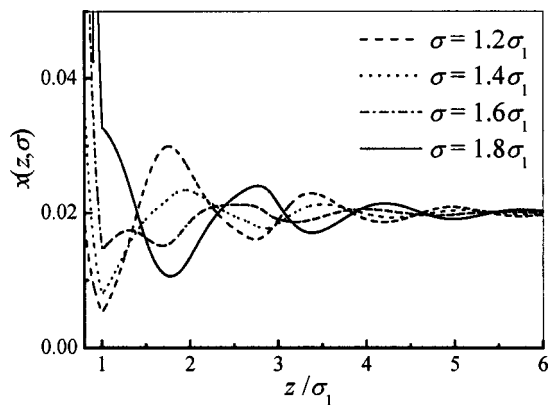


FIG. 9. Local concentrations of four fractions of uniform polydisperse hard spheres near a hard wall at the bulk density $\rho_{0b}\sigma_1^3=0.24$.

asymmetric hard-sphere mixtures. Furthermore, it is capable of predicting the structures of hard-sphere fluid confined in different geometries.³¹

The present theory predicts the density profiles of polydisperse hard-sphere mixtures with uniform distribution of diameters near a hard wall in excellent agreement with the Monte Carlo simulation results. It is also feasible to describe the structure of polydisperse hard-sphere mixture with nonlinear distribution in a broader interval. It shows significant size segregations for uniformly polydispersed hard spheres near the wall. The systems considered in this work represent simple models of colloidal dispersions in the presence of an impenetrable surface relevant to many practical applications. These systems can also be used as a reference for developing perturbation theory to study more complex systems such as electric double layer,³⁴ associating fluids,³⁵ and polymers³⁶ confined in various geometries. In the future work, we intend to extend the present theory to polydisperse systems containing particles with a continuous distribution of other parameters such as charge or chemical composition.

ACKNOWLEDGMENT

This work is supported by the National Natural Science Foundation of China (Project Grant No. 20376037).

¹H. Xu and M. Baus, *J. Chem. Phys.* **118**, 5045 (2003).

²J. P. Hansen and I. R. McDonald, *Theory of Simple Liquids*, 2nd ed. (Academic, London, 1986).

³J. K. Percus and G. J. Yevick, *Phys. Rev.* **110**, 1 (1958).

⁴R. Evans, in *Fundamentals of Inhomogeneous Fluids*, edited by D. Henderson (Dekker, New York, 1992).

⁵I. Pagonabarraga, M. E. Cates, and G. J. Ackland, *Phys. Rev. Lett.* **84**, 911 (2000).

⁶J. L. Lebowitz, *Phys. Rev. A* **133**, 895 (1964); A. König and N. W. Ashcroft, *Phys. Rev. E* **63**, 041203 (2001); M. Yasutomi and M. Ginoza, *J. Phys.: Condens. Matter* **12**, L605 (2000); C. Caccamo, G. Pellicane, R. Ricciari, and G. Faggio, *ibid.* **12**, 2613 (2000); A. Santos, S. B. Yuste, and M. L. de Haro, *J. Chem. Phys.* **117**, 5785 (2002).

⁷F. Lado, *Phys. Rev. E* **54**, 4411 (1996); *J. Chem. Phys.* **108**, 6441 (1998); S. Leroch, G. Kahl, and F. Lado, *Phys. Rev. E* **59**, 6937 (1999); B. D'Aguzzo and R. Klein, *ibid.* **46**, 7652 (1992).

⁸J. J. Salacuse and G. Stell, *J. Chem. Phys.* **77**, 3714 (1982); J. A. Gualtieri, J. M. Kincaid, and G. Morrison, *ibid.* **77**, 521 (1982); Y. V. Kalyuzhnyi and G. Kahl, *ibid.* **119**, 7335 (2003).

⁹P. Bryk, A. Patrykiewicz, J. Reszko, and S. Sokolowski, *J. Chem. Phys.* **111**, 6047 (1999).

¹⁰C. N. Patra and S. K. Ghosh, *J. Chem. Phys.* **117**, 8933 (2002).

¹¹C. N. Patra and S. K. Ghosh, *J. Chem. Phys.* **118**, 3668 (2003).

¹²O. Pizio, A. Patrykiewicz, and S. Sokolowski, *Mol. Phys.* **99**, 57 (2001).

¹³Y.-X. Yu and J. Z. Wu, *J. Chem. Phys.* **117**, 10156 (2002).

¹⁴C. N. Patra and S. K. Ghosh, *J. Chem. Phys.* **106**, 2762 (1997).

¹⁵D. W. Oxtoby, *Nature (London)* **347**, 725 (1990).

¹⁶T. V. Ramakrishnan and M. Yussouff, *Phys. Rev. B* **19**, 2775 (1979); D. W. Oxtoby and A. D. J. Haymet, *J. Chem. Phys.* **76**, 6262 (1982); T. H. Yoon and S. C. Kim, *Phys. Rev. E* **58**, 4541 (1998); N. Choudhury and S. K. Ghosh, *J. Chem. Phys.* **110**, 8628 (1999).

¹⁷P. Tarazona, *Phys. Rev. A* **31**, 2672 (1985); P. Tarazona, *ibid.* **32**, 3148 (1985).

¹⁸W. A. Curtin and N. W. Ashcroft, *Phys. Rev. A* **32**, 2909 (1985).

¹⁹T. F. Meister and D. M. Kroll, *Phys. Rev. A* **31**, 4055 (1985); A. R. Denton and N. W. Ashcroft, *ibid.* **39**, 4701 (1989); X. C. Zeng and D. W. Oxtoby, *ibid.* **41**, 7094 (1990); R. Leidl and H. Wagner, *J. Chem. Phys.* **98**, 4142 (1993).

²⁰Y. Rosenfeld, *Phys. Rev. Lett.* **63**, 980 (1989).

²¹E. Kierlik and M. L. Rosinberg, *Phys. Rev. A* **42**, 3382 (1990).

²²Z. Tan, U. M. B. Marconi, F. van Swol, and K. E. Gubbins, *J. Chem. Phys.* **90**, 3704 (1989).

²³A. R. Denton and N. W. Ashcroft, *Phys. Rev. A* **44**, 8242 (1991).

²⁴S.-C. Kim, C. H. Lee, and B. H. Seong, *Phys. Rev. E* **60**, 3413 (1999).

²⁵C. N. Patra, *J. Chem. Phys.* **111**, 6573 (1999).

²⁶F. J. Rogers and D. A. Young, *Phys. Rev. A* **30**, 999 (1984).

²⁷S.-C. Kim and S. H. Suh, *Mol. Phys.* **99**, 81 (2001).

²⁸P. Bryk, A. Patrykiewicz, and S. Sokolowski, *Mol. Phys.* **99**, 1709 (2001).

²⁹R. Roth, R. Evans, A. Lang, and G. Kahl, *J. Phys.: Condens. Matter* **14**, 12063 (2002).

³⁰T. Boublik, *J. Chem. Phys.* **53**, 471 (1970); G. A. Mansoori, N. F. Carnahan, K. E. Starling, and T. W. J. Leland, *ibid.* **54**, 1523 (1971).

³¹Y.-X. Yu and J. Z. Wu, *J. Chem. Phys.* **119**, 2288 (2003).

³²Y. Rosenfeld, M. Schmidt, H. Lowen, and P. Tarazona, *Phys. Rev. E* **55**, 4245 (1997); P. Tarazona, *Phys. Rev. Lett.* **84**, 694 (2000).

³³M. Sindelka and T. Boublik, *Fluid Phase Equilib.* **143**, 13 (1998).

³⁴C. N. Patra and S. K. Ghosh, *J. Chem. Phys.* **117**, 8938 (2002); Y. X. Yu, J. Z. Wu, and G.-H. Gao, *ibid.* **120**, 7223 (2004).

³⁵Y. X. Yu and J. Z. Wu, *J. Chem. Phys.* **116**, 7094 (2002); S. Tripathi and W. G. Chapman, *ibid.* **119**, 12611 (2003); A. Patrykiewicz, O. Pizio, L. Pusztai, and S. Sokolowski, *Mol. Phys.* **101**, 2219 (2003).

³⁶Y. X. Yu and J. Z. Wu, *J. Chem. Phys.* **117**, 2368 (2002); M. B. Sweatman, *J. Phys.: Condens. Matter* **15**, 3875 (2003); J. Forsman and C. E. Woodward, *J. Chem. Phys.* **120**, 506 (2004).